ETH
Eidgenössische Technische Hochschule Zürich
Swiss Federal Institute of Technology Zurich

RSL Robotic Systems Lab
Prof. Dr. Marco Hutter

Bachelor Thesis

Minimal on Wheels

Spring Term 2024

Supervised by:
Filip Bjelonic
Victor Klemm

Author:
Niclas Scheuer

Declaration of Originality

I hereby declare that the written work I have submitted entitled

Minimal on Wheels

is original work which I alone have authored and which is written in my own words.[1]

Author(s)

Niclas	Scheuer

Student supervisor(s)

Filip	Bjelonic
Victor	Klemm

Committee members(s)

EMPTY	EMPTY

Supervising lecturer

Marco	Hutter

With the signature I declare that I have been informed regarding normal academic citation rules and that I have read and understood the information on 'Citation etiquette' (`https://www.ethz.ch/content/dam/ethz/main/education/rechtliches-abschluesse/leistungskontrollen/plagiarism-citationetiquette.pdf`). The citation conventions usual to the discipline in question here have been respected.

The above written work may be tested electronically for plagiarism.

Place and date	Signature

[1] Co-authored work: The signatures of all authors are required. Each signature attests to the originality of the entire piece of written work in its final form.

Intellectual Property Agreement

The student acted under the supervision of Prof. Hutter and contributed to research of his group. Research results of students outside the scope of an employment contract with ETH Zurich belong to the students themselves. The results of the student within the present thesis shall be exploited by ETH Zurich, possibly together with results of other contributors in the same field. To facilitate and to enable a common exploitation of all combined research results, the student hereby assigns his rights to the research results to ETH Zurich. In exchange, the student shall be treated like an employee of ETH Zurich with respect to any income generated due to the research results.
This agreement regulates the rights to the created research results.

1. Intellectual Property Rights

1. The student assigns his/her rights to the research results, including inventions and works protected by copyright, but not including his moral rights ("Urheberpersönlichkeitsrechte"), to ETH Zurich. Herewith, he cedes, in particular, all rights for commercial exploitations of research results to ETH Zurich. He is doing this voluntarily and with full awareness, in order to facilitate the commercial exploitation of the created Research Results. The student's moral rights ("Urheberpersönlichkeitsrechte") shall not be affected by this assignment.
2. In exchange, the student will be compensated by ETH Zurich in the case of income through the commercial exploitation of research results. Compensation will be made as if the student was an employee of ETH Zurich and according to the guidelines "Richtlinien für die wirtschaftliche Verwertung von Forschungsergebnissen der ETH Zürich".
3. The student agrees to keep all research results confidential. This obligation to confidentiality shall persist until he or she is informed by ETH Zurich that the intellectual property rights to the research results have been protected through patent applications or other adequate measures or that no protection is sought, but not longer than 12 months after the collaborator has signed this agreement.
4. If a patent application is filed for an invention based on the research results, the student will duly provide all necessary signatures. He/she also agrees to be available whenever his aid is necessary in the course of the patent application process, e.g. to respond to questions of patent examiners or the like.

2. Settlement of Disagreements

Should disagreements arise out between the parties, the parties will make an effort to settle them between them in good faith. In case of failure of these agreements, Swiss Law shall be applied and the Courts of Zurich shall have exclusive jurisdiction.

Place and date	Signature

Contents

Preface

The journey to writing this thesis began with a fascination with mobile robotics and a personal passion for working on my own small quadruped robot Petoi Bittle. This thesis centers on "Minimal", a small quadruped robot I have modified to allow both walking and driving motion. My interest in hybrid legged-wheeled systems, an exciting avenue in robotic mobility research, have inspired me to pursue this project.

The primary objective of the study was to explore the benefits of adding motorized wheeled to the quadruped platform "Minimal". In this regard, the thesis initially started with formulating the design goals of the thesis, which then progressed into motor and wheel selection, CAD design, and production. Additionally, driving and walking policies were created in a massively-parallelized simulation and subsequently implemented on the robot using a ROS2 framework, culminating in the integration of all hardware components.

Throughout this project, I was forunate to receive abundant support from the Robotics Systems Lab (RSL) at ETH Zürich. I would like to extend my heartfelt gratitude to my supervisors Filip Bjelonic and Victor Klemm, as well as to Prof. Dr. Marco Hutter and Fabian Tischhauser, for their guidance and support.

I am also deeply grateful to my family and close friends for their support and encouragement along this journey.

I hope that the findings of this research contribute to the advancement and accessibility of mobile robotics, and inspires further innovation in the field.

Abstract

This thesis explores the implementation of motorized wheels into the feet of a small quadruped robot named "Minimal" to augment its mobility. I began by formulating the design and mobility requirements of "Minimal on Wheels" by using the parameters of the "Minimal" robot. Motor requirements included the need for sufficient torque to overcome small obstacles and inclines, low mass, and low power consumption. The newely motorized lower legs for "Minimal" were designed to be robust, lightweight, and modular, as well as routing all the cables inside the leg itself. The shank can be produced on a commercial 3D-printer in under 3 hours, enabling rapid prototyping. I also designed and 3D-printed wheels using TPU (thermoplastic polyurethane), offering a quick and versatile approach for evaluating different designs.
Minimal on Wheels was implemented as a URDF file, complete with all STL files, to facilitate accurate implementation in simulation. RSL's legged gym training environment was used to create several simple walking and driving policies, which were then validated in real-world scenarios. The work provides a foundation for future studies on advanced hybrid control policies and hardware optimizations.

Symbols

Symbols

ϕ, θ, ψ	roll, pitch and yaw angle
b	gyroscope bias
Ω_m	3-axis gyroscope measurement

Indices

x	x axis
y	y axis

Acronyms and Abbreviations

RSL	Robotics Systems Lab at ETH Zürich
IMU	Inertial Measurement Unit
HAA	Hip Abduction/Adduction
HFE	Hip Flexion/Extension
KFE	Knee Flexion/Extension
PLA	Polylactic Acid
TPU	Thermoplastic Polyurethane
GRU	Gated Recurrent Unit
PPO	Proximal Policy Optimization
DD	Direct Drive
SEA	Series Elastic Actuator
FEA	Finite Element Analysis
PCB	Power Control Board
ROS	Robot Operating System
URDF	Unified Robotics Description Format
STL	Sterolithography file format
DoF	Degrees of Freedom
DC	Direct Current
AC	Alternating Current
BLDC	Brushless Direct Current
MOSFET	Metal-oxide-semiconductor Field-effect transistor

MLP Multilayer perceptron

Chapter 1

Introduction

1.1 Motivation

Significant advancements in computation power and control algorithms have allowed mobile robotics to become as prevalent as never before. Within this broader field, legged robotics has emerged as a particularly exciting area of research, drawing inspiration from biological systems [1]. Legged robots exhibit promising capabilities such as object manipulation [2], the ability to carry substantial loads, and the proficiency to navigate difficult terrain [3] [4], making them ideal for a wide range of applications.
An emerging subfield within legged robotics is the development of wheeled-legged robots, which combine the benefits of both driving and walking. These hybrid systems achieve rapid locomotion on flat surfaces using wheels, while retaining the ability to overcome larger obstacles through climbing with their legs [5]. Hybrid legged-wheeled robots benefit from this dual functionality by adapting to a variety of terrains and operational scenarios.
Inspired by these advancements, we decided to configure Minimal, a small quadruped robot, to incorporate motorized wheels.

1.2 Minimal

Minimal is a lightweight robotic platform developed at the Robotics Systems Lab at ETH Zürich for research. It is a 12-DoF quadruped controlled by a Nvidia Jetson [6] and is internally powered by 18V DC power. Twelve T-Motor MN4006 [7] motors actuate the HAA, HFE, and KFE joints using ball screws. Minimal is a compact platform, measuring 100mm x 100mm x 100mm folded and coming in at 5kg.

1.3 Review of Existing Hybrid Systems

The addition of motorized wheels into legged robots has evolved in various forms of robots with varying applications. Bipedal robots such as Ascento [8], Tencent's Ollie [9], and Boston Dynamics' Handle [10] balance on two wheels while using actuated legs to overcome obstacles such as stairs and ramps. These robots are particularly apt at efficiently navigating copmlex environments such as for logistics and facility management.
Quadrupedal wheeled-legged robots such as ANYmal on Wheels [11], Maera [12], or Unitree's B2-W [13] combine the stability and load-carrying capabilites of quadruped platforms with the practicality of wheeled locomotion. Robots such as these can use

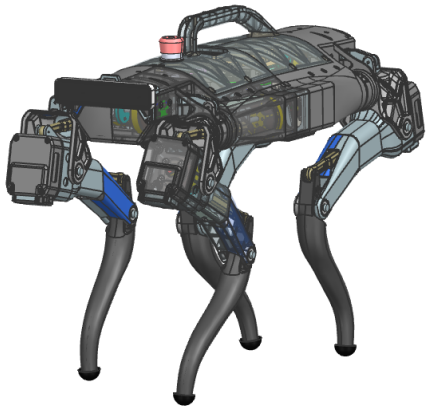

Figure 1.1: Minimal.

extensive sensor loadouts to adaptively navigate complex urban environments [14], with possible applications including delivery, maintenance, and emergency rescue.
The control algorithms running wheeled-legged systems are of particular interest to researchers, such as the effect of cross-coupling between degrees of freedom, and prospects of combined driving-walking policies. Furthermore, the integration of hardware components for hybrid systems is not trivial. Motorized wheels on quadruped platforms require large torques, achieving precise position control, and maintaining low mass.

1.4 Scope

The thesis explores the integration of wheels into the quadruped robot "Minimal" to create a verstaile wheeled-legged robot. The objectives of the research include achieving fast and efficient movement using the new hybrid platform, while maintaining a modular design for easy modification.
Several research questions are addressed, such as method of wheel integration, the motor choice, as well as how deep learning and physics simulations can be used to develop efficient driving and walking policies.
The study focuses solely on the quadruped robot "Minimal" and is limited to the design, simulation, and validation phases, without extensive field testing.

Chapter 2

Motor Choice

2.1 Hardware Requirements

Minimal on Wheels should be a versatile and agile platform. Given Minimal's lightweight construction, a wheeled Minimal can be high accelerations and top speeds. Nevertheless, it should also be capable of traversing uneven and sloped terrain in driving mode.

2.1.1 Primary Requirements

- **Speed and Terrain Negotiation**: Minimal must be capable of moving at 1 m/s while:
  - Negotiating an uphill slope of 10 degrees.
  - Crossing uneven terrain with a rolling resistance coefficient of $\mu = 0.1$.
- **Acceleration**: Minimal should be capable of accelerations of 1 m/s^2 or greater.
- **Torque Requirements**: The wheel motors must provide sufficient torque to use a 0.1m radius wheel and achieve the above tasks.
- **Power Compatibility**: The motor must be compatible with the existing 18V power supply and be as power-efficient as possible.
- **Weight Considerations**: The motor and wheel should be as light as possible to maintain the leg's range of motion.

2.2 Motor Selection

The motor type is a critical decision for the design of Minimal on Wheels. As Minimal internally runs on 18V DC power, we restrict ourselves to the use of DC motors.

2.2.1 Brushed vs. Brushless Motors

Brushed DC Motors
Brushed DC motors are inexpensive and simple to control. They also benefit from high starting torque. However, they have limited lifespans due to the frictional degradation of the brushes, which also negatively affects the efficiency of the motor. Since Minimal is to use the motors for wheeled locomotion, especially over longer distances, brushed motors are deemed unfavorable for this task.

Brushless DC Motors
Brushless DC motors are more expensive than brushed DC motors, but eliminate the mechanical brushes, resulting in less wear and maintenance. Consequently, they benefit from high efficien- cies, high lifespans, and effective control strategies. This is the type of motor selected for Minimal on Wheels.

2.2.2 Direct Drive vs. Quasi-Direct Drive

Direct Drive (DD) Configuration
This type of configuration refers to a setup where the BLDC (Brushless DC) motor is directly connected to the load (wheel) without any additional mechanical components.
Direct drive systems benefit from simple construction, low mass, low mechanical impedance, and high reliability. In addition, the absence of gears or other mechanical components between the motor and the wheel allows for more transparent torque readouts.
However, direct drive systems are limited in their torque output. Without the benefit of mechanical advantage, the torque transferred to the wheel is restricted to the torque directly produced by the motor.

Quasi-Direct Drive (QDD) Configuration
Quasi-direct drive (QDD) systems use a mechanical transfer stage between the BLDC motor and the load, such as a single-stage planetary reduction gear.
The primary advantage of a quasi-direct drive system is the ability to achieve a high torque output through gear ratios.
However, the addition of a gear train imposes several constraints on Minimal's capabilities. These include increased play and time delay in teh gear train, as well as increased inertia at the joint.
Additionally, since the wheel is attached to the end of teh leg and acts as it's foot during walking, it is subjected to frequent and strong shocks, such as during climbing and descent. Consequently, the motor and gear train must be correctly dimensioned to resist these forces over a longer period of time, something that is more difficult to validate with a complex QDD motor. The methods used to migitate these disturbances are covered in 3.2.2.

Series Elastic Actuators (SEA)
Series Elastic Actuators (SEA) are a popular actuation choice for robotic applications [15] since being introduced in 1995 [16]. They combine a motor, gears,

and a compliant mechanism to provide high fidelity force control in a variety of applications.
However, SEA systems are the heaviest and most copmlex of the three configurations. Non-linearities in the elastic elements and the subsequent bandwidth limitations make control more challenging.

Decision
Owing to their lightweight construction and commercial availability, direct drive (DD) motors were decided for Minimal on Wheels. In the following sectios, the torque requirements are calculated, and various direct drive motors are evaluated against these requirements.

2.2.3 Torque Calculation

As defined by the requirements, Minimal on Wheels should be capable of ascending a 10 degree slope at $1m/s^2$ in addition to navigating terrain with a rolling resistance coefficient of $\mu = 0.1$.
A distinctive part of the problem formulation is the fact that Minimal, as a hybrid quadruped, can have between $n = 2 - 4$ wheels in contact with the ground. This increases the torque requirements.

Parameters

n Number of wheels in contact with the ground, which can be 2,3, or 4
m Inflated mass of Minimal 5 kg
$a_{\mathbf{ref}}$ Acceleration of Minimal, 1 m/s^2
$r_{\mathbf{wheel}}$ Radius of the wheel, 0.1 m
θ Inclination of the ground, 10°

The mass of the unmodified Minimal robot is 3.828 kg. To account for the additional mass of wheels, motors, and electronics, it has been inflated to 5kg.

Calculation
Starting from a force equilibrium along the slope of the incline and using no-slip condition:

$$\sum_{i=1}^{n} F_{wheels} = \sum F_{external} \tag{2.1}$$

$$n \cdot F_{wheel} = F_{inertia} + F_{gravity} + F_{rolling} \tag{2.2}$$

$$n \cdot \frac{T_{motor}}{r_{wheel}} = ma_{ref} + mg\cos(\theta) + \mu mg\sin(\theta) \tag{2.3}$$

$$T_{motor} = \frac{r_{wheel}m}{n} \cdot (a_{ref} + g\sin(\theta) + \mu g\cos(\theta)) \tag{2.4}$$

Table 2.1: Torque Requirements for Different Slopes and Accelerations

Torques (Nm)	$n = 4$			$n = 2$		
	$a_{ref} = 0.5$	$a_{ref} = 1$	$a_{ref} = 2$	$a_{ref} = 0.5$	$a_{ref} = 1$	$a_{ref} = 2$
$\theta = 0°$	0.185	0.2475	0.373	0.370	0.495	0.745
$\theta = 5°$	0.292	0.354	0.479	0.583	0.708	0.958
$\theta = 10°$	0.396	0.459	0.584	0.792	0.917	1.167

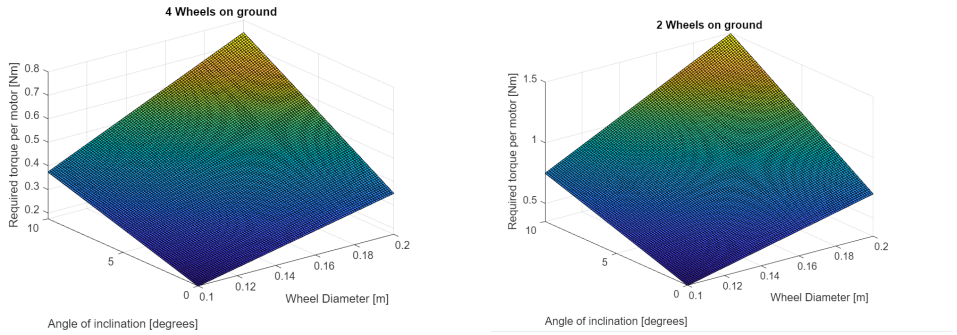

Figure 2.1: Effect of wheel diamater and inclindation on torque requirements.

Based on these calculations, each motor should be capable of producing at least ≈ 1.5Nm to fulfill the driving specifications outlined earlier.

2.2.4 Motor Comparison

In this section, I compared several motors from the manufacturers 'T-Motor' and 'I-Flight' with the necessary compatibility with Minimal's 18V power supply. The full list of all motors and specifications can be found in Table B.1. Data was collected from the T-Power [17] and iFlight [18] websites respectively.
Of particular importance is the maximum torque of the motor, its weight, and its maximum current draw. These are displayed in Figure.

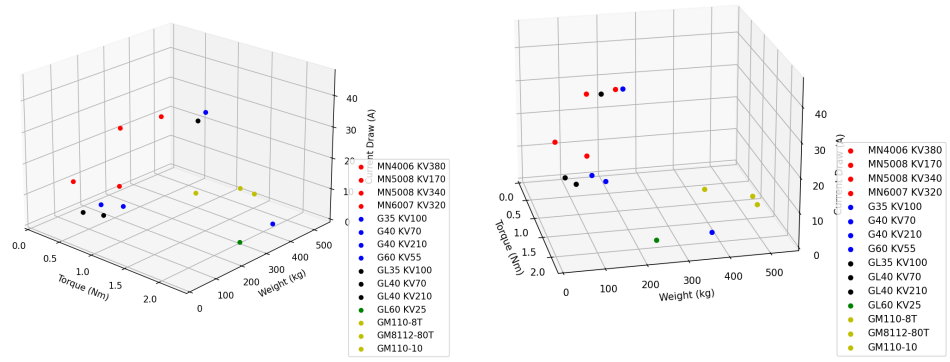

Figure 2.2: Plots of motor characteristics.

Visible in the plots are patterns along manufacturers series of motors, such as the 'Antigravity MN' series of drone motors from 'T-Motor' being particularly lightweight but characterized by low torque and high power consumption. Among these motors, the 'T-Motor GL60 KV25' outrunning gimbal motor stands out due to its balance across multiple factors:

1. **Torque:** The motor exhibits an impressive maximum torque of around 2.25Nm.
2. **Current Draw:** The GL60 KV25 consumes only 4.2 Amperes at maximum power, permitting long driving durations
3. **Weight:** At 230g, the weight of the motor is within acceptable limits for the robot's design. This is further validated in Appendix A.1.

2.3 Motor Validation

2.3.1 Simulink Setup

In order to validate the performance of the selected 'GL60 KV25', I created a Simulink program that uses the motor mapping of the 'GL60' motor available online and tests it over terrain.

Figure 2.3: Motor Mapping accessed from the T-Motor website [19]

Rearranging equation (2.4) permits us to find the resultant acceleration given a motor torque. In order to avoid the non-linearities that arise from the friction term as Minimal changes direction, it has been appended with a sigmoid function. Furthermore, motor efficiency ϵ and a safety factor S_F have been added to the equation.

$$a_{actual} = \frac{\epsilon \cdot \tau_{motor} \cdot n}{M \cdot r \cdot S_F} - g\sin(\theta) - \mu g\cos(\theta) \cdot \left[\frac{2}{1+\exp(-10v)} - 1\right] \tag{2.5}$$

Using this equation, and information about the number of wheels on ground (n), the inclination and resistance of the immediate terrain (θ, μ), the wheel radius (r), we are able to simulate the robot traversing a terrain map. All four motors are controlled in a group, not individually.

At any given time, a PID controller takes the error between the intended velocity v_{ref} and the true velocity v_{actual} to regulate the current into the motors, which is then fed through the motor mapping to find the output torque.

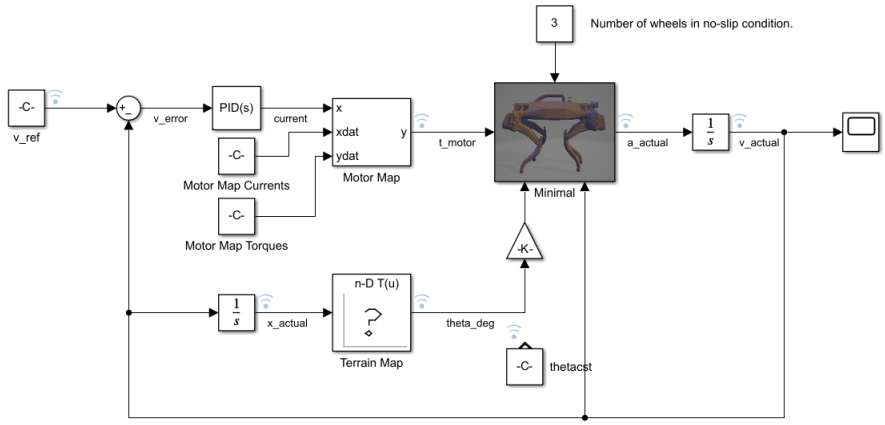

Figure 2.4: Overview of the Simulink Environment

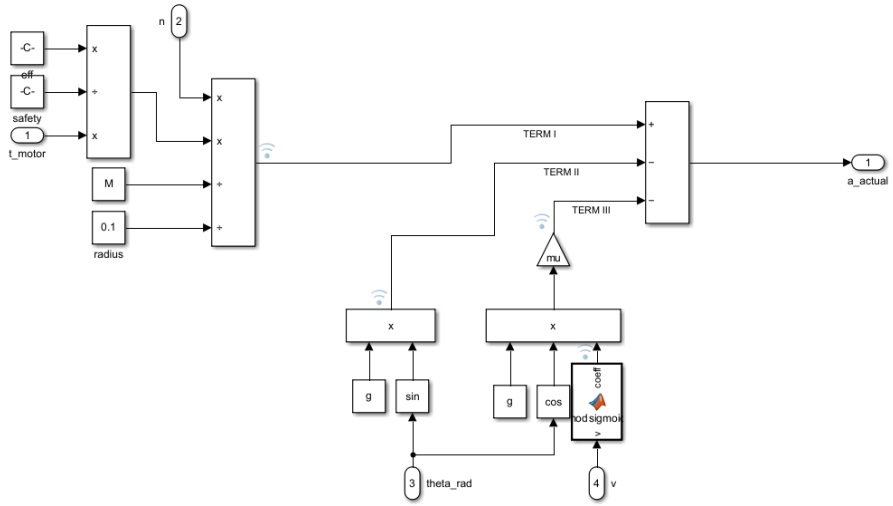

Figure 2.5: Determining acceleration from input torques using Equation (2.5)

The simulation runs at real time and various parameters can be changed at runtime using a control panel, including:

- Commanded reference velocity v_{ref}
- Wheel radius r
- Inclination of terrain θ
- Number of wheels in ground contact n
- Coefficient of rolling friction μ
- Motor efficiency ϵ
- Safety factor S_F

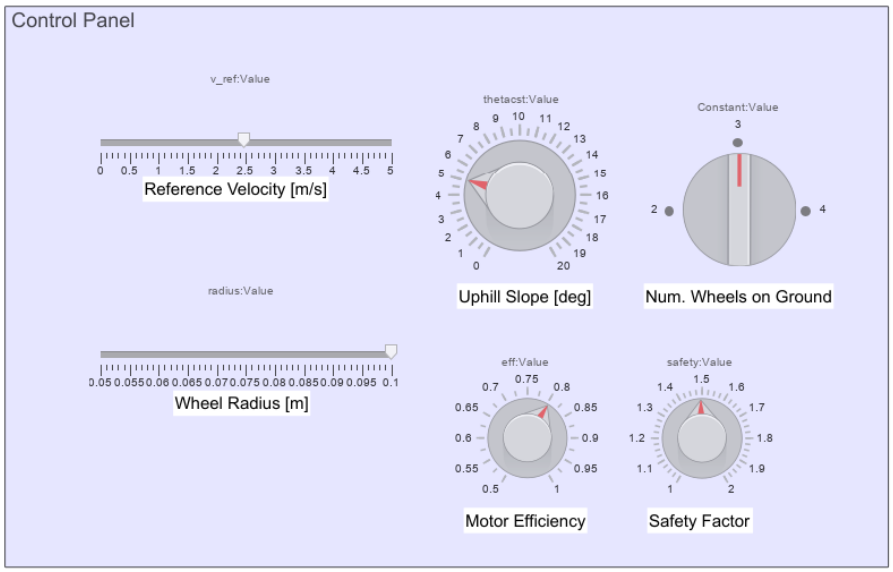

Figure 2.6: Control Panel for Simulink

2.3.2 Results

Minimal on Wheels with the 'GL60' motors performs well over a variety of drive and terrain configurations, including:

- Reference speed changes between $0.5m/s$ and $2.0m/s$
- Wheel radius changes from 0.05m to 0.1m
- Inclinations ranging from 0 deg. to 15 deg.
- Driving on 2 to 4 wheels
- Coefficients of friction between 0.02 and 0.1
- Motor efficiencies between 0.7 and 1.0

An excerpt of the results is summarized below. In Figure 2.7, Minimal is commanded to accelerate to $1m/s$ from standstill on an incline of $\theta = 10$ deg. and $\mu = 0.1$. Minimal first performs this task with all four wheels on the ground, then with just two wheels on the ground.

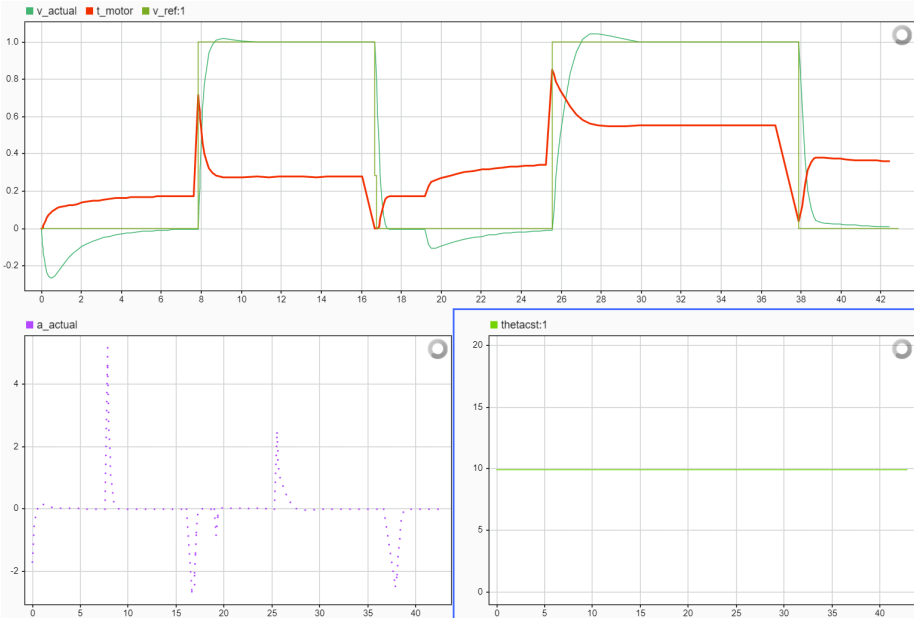

Figure 2.7: Minimal accelerates up a 10 degree slope. Note the 'bump' just before the 20-second mark, when it switches from 4-wheel drive to 2-wheel drive.

As can be seen from the plot, Minimal confidently meets the design requirements using the 'GL60 KV25' motor. It tracks the reference velocity well, achieving accelerations up to $4m/s^2$, while not exceeding 1.0Nm.

Chapter 3

Wheel and Leg Design

This chapter presents the design process for the wheels, legs, and electronic configuration for Minimal on Wheels.

3.1 Wheel Design

3.1.1 Design Requirements

Minimal should use wheels that are easy-to-replace, lightweight, and are suitable for it's driving and walking applications. In this regard, several design requirements were formulated:

1. **Replaceable Design:** The wheel should be able to be replaced using basic tools in the field.
2. **Longevity:** For this proof of concept, the wheel should function reliably for at least 10 operational cycles, given that Minimal's battery life is approximately 1 hour under normal operation.
3. **Damping:** Minimal uses the wheels as it's feet during walking operation. Adding damping to the wheels reduces the resultant forces on the axle and motor mount.
4. **Weight:** Minimal's wheels should be as lightweight as possible without compromising durability and performance.
5. **Rounded Rolling Surface:** Given the legged configuration of Minimal, which allows the HAA joint to operate at various angles, the wheel may be used at a variety of camber angles, as illustrated in Fig. 3.1. Therefore, the rolling surface of the wheel should be rounded along the roll axis.
6. **Dimensions:** The wheel should have a diameter between 100 and 200 millimeters, and the width should not exceed 30 millimeters.

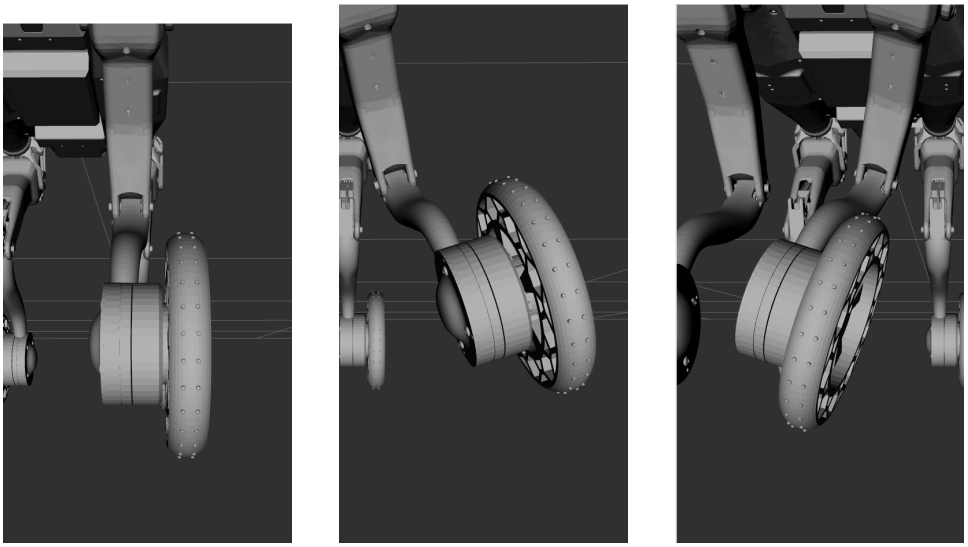

Figure 3.1: Minimal may use the wheels at a variety of camber angles.

3.1.2 Wheel Selection and Design

During the design phase, several types of wheels were evaluated. Initial considerations included:

- **E-Scooter Wheels**: While fitting the size criteria, these wheels are dimensioned to sustain loads in excess of 80kg. As a result, they are heavy and provide close to no damping for a robot as lightweight as Minimal.
- **RC Car Wheels**: These wheels also met the size requirements and are readily commercially available. However, they failed to fulfill several other design requirements. Most RC wheels consist of a plastic shell with a rubber layer, offering excellent friction but inadequate damping. Additionally, many RC wheels lack the rounded rolling surface specifically required by Minimal. Furthermore, RC wheels often utilize varying attachment standards, making wheel interchangeability cumbersome and necessitating adapters, which would increase the overall weight.

Given these limitations, the decision was made to design and 3D-print custom wheels using Thermoplastic Polyurethane (TPU). TPU was selected for its combination of high friction, exceeding conventional rubber materials [20], flexibility, low density, and durability [21].

Using Siemens NX (Siemens Digital Industries Software) a custom wheel of diameter 120mm and width 20mm was designed. It exploits TPU's flexibility by using an internal honeycomb pattern inspired by Resilient Technologies NPT (non-pneumatic tire) [22]. The tire features 60 small studs along the surface to increase grip.

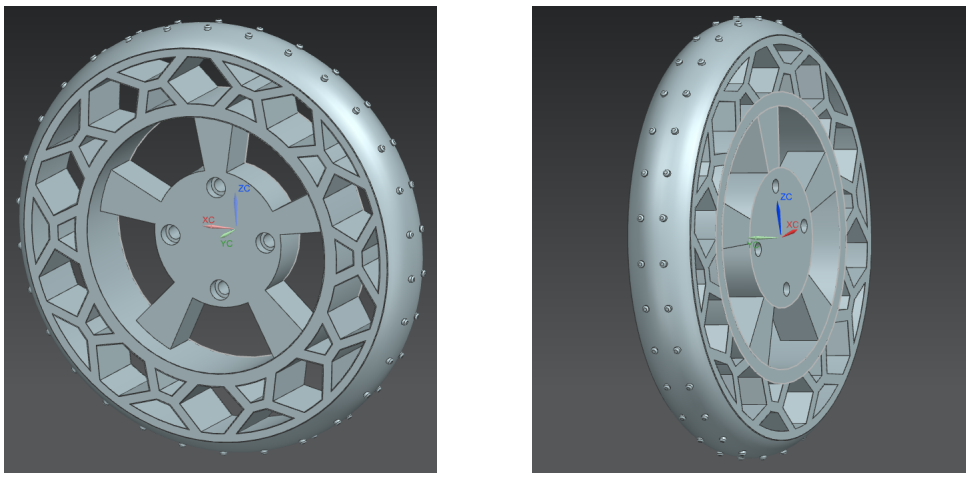

Figure 3.2: CAD Design of the TPU wheel.

3.1.3 FEM Validation

In order to verify the longevity of the TPU wheel under regular operating conditions, a Finite Element Analysis (FEA) was conducted using Siemen's NX built-in analysis tool.
3D-printed components, including the TPU wheel, often feature an internal infill structure that significantly affects their mechnical properties. The density of the infill, as well as the pattern can influence the strength, flexibility, and weight of the 3D-printed part. The following factors were considered:

- **Infill Density:** The percentage of internal volume that is filled with TPU material. Increasing this percentage increases the weight and strength of the wheel.
- **Infill Pattern:** The geometric pattern of the infill inside the component. Common patterns include honeycomb, grid, or gyroid. Internal load distribution is affected by the pattern choice.
- **Layer Height:** The thickness of each individual layer of material deposited during the 3D printing process. [ADD MORE]

For Minimal's TPU wheels, a 20% infill with grid pattern and a layer height of 0.2mm was used.

Simulation Process
To accurately simulate the TPU wheel, the CAD model was updated with a 20% internal grid infill. The material properties of TPU, sourced from MatWeb [21], were imported into Siemens NX's Nastran Solver. The wheel and its internal infill structure were meshed using quadratic tetrahedral elements (TETRA10) with a maximum element size of 0.2 mm. A radial load of 20 N was applied to the surface of the wheel, corresponding to an equivalent weight of approximately 2 kg per wheel. Fixed constraints were applied at the four screw holes located at the center of the wheel.

Results
The results of the simulation are shown in Figures 3.3 and 3.4 below:

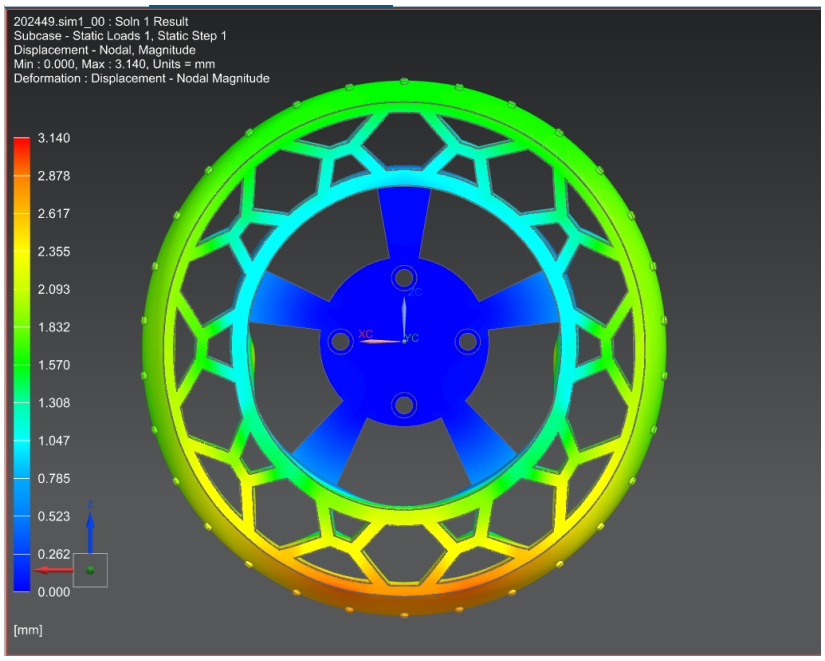

Figure 3.3: Displacement results of the FEA simulation.

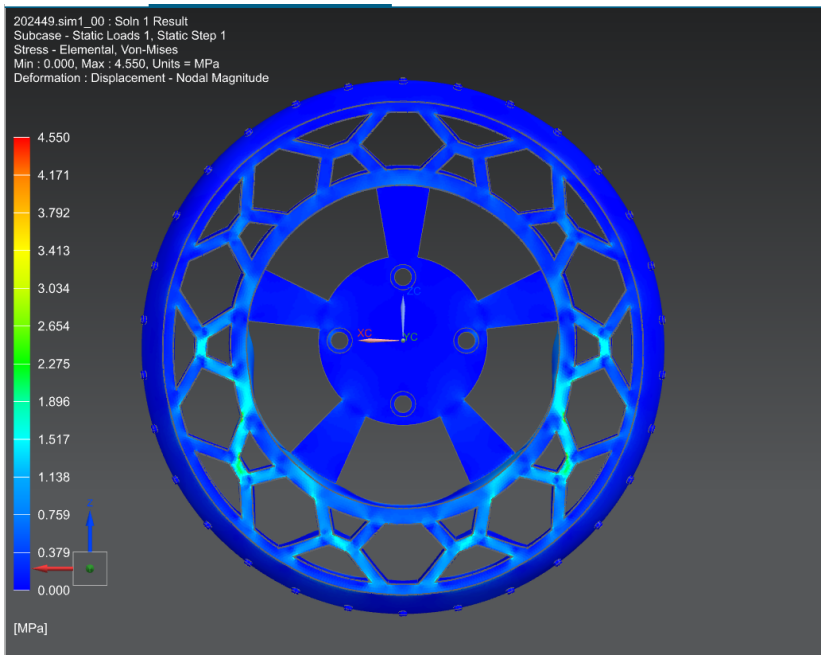

Figure 3.4: Stress results of the FEA simulation.

According to the FEA, the maximum elemental stress imparted on the wheel is 4.55 MPa. Research by Wang et. al. [23] indicates that the fatigue limit of Thermoplastic

Polyurethane is 10.25 MPa, suggesting the wheel may, at least internally, endure an infinite number of cycles without experiencing fatigue failure. Nevertheless, other factors such as wear and friction also play a role in the wheel's longevity.
This preliminary analysis shows promising results regarding the wheel's durability.

3.1.4 Production

A Creality Ender V3 KE (Shenzhen Creality 3D Technology Co., Ltd.) was used to print the wheels using Creality "CR-TPU" material. As mentioned in 3.1.3, a 20% grid infill pattern was used with a 0.2mm layer height. Nozzle and bed temperature were set to 210 and 60 degrees respectively.
Figure 3.5 shows one of the TPU wheels being printed, while Figure 3.6 shows a completed wheel.

Figure 3.5: Wheel being printed in black TPU.

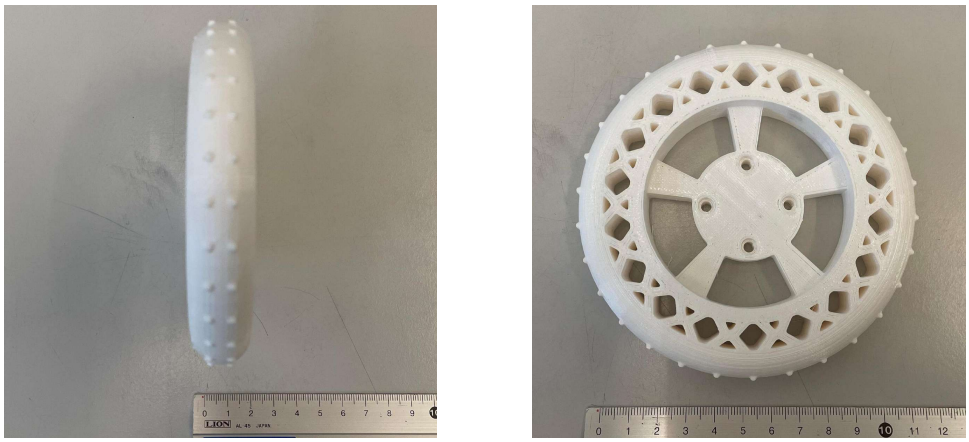

Figure 3.6: Prototype wheel printed in white TPU.

3.2 Leg Design

3.2.1 Design Requirements

In order to fit the motors and wheels onto Minimal, the leg configuration has to be modified. In this regard, I changed the design of the lower leg, hencefore referred to as "shank". I set myself several design requirements for this task:

1. **Part Count:** The new shank and wheel attachment should consist of as few parts as possible, including the motor.
2. **Encoder Compatibility:** In order to effectively perform position and velocity control, an encoder mount should be available and protected from the elements.
3. **Weight:** The newly-designed shank should be as lightweight as possible.
4. **Modularity:** Minimal's wheeled shank should be practical to use and easy to replace.
5. **Hybrid Motion:** The shank enables both walking and driving motions.

3.2.2 CAD Iterations

Similarly to the wheels, all CAD designs were modelled in Siemens NX (Siemens Digital Industries Software). Additionally to the above requirements, geometries had to be simple to be suited for 3D-printing. The use of threaded inserts greatly facilitated assembly and enhanced the construction's robustness. 3D-printing and rapid prototyping facilitated the creation and evaluation of three design iterations.

Iteration I
Iteration I was characterized by a heavy design with numerous parts, as shown in Figure 3.7. The inner axle employed two dedicated shaft-hub connections, significantly increasing part count and complexity. Apart from difficulties 3D-printing tight tolerances to fit the shaft-hub connections, the size of the shaft meant the encoder had to be installed further from the shank, increasing the weight of the build. A cover was included around the construction to provide additional protection, but also increased weight and complexity.

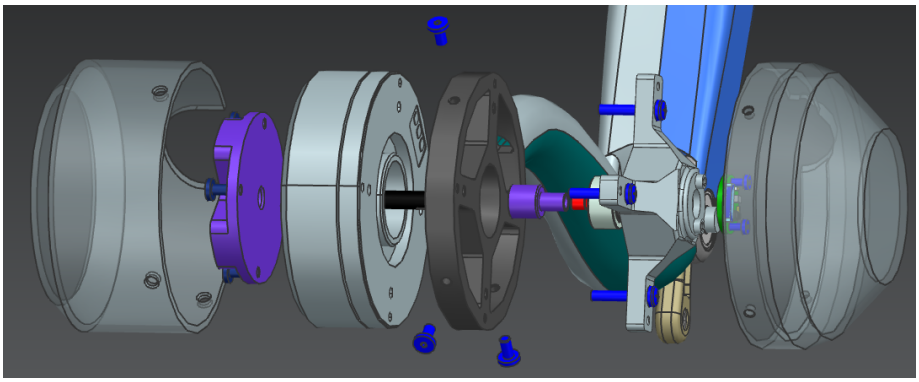

Figure 3.7: Exploded view of the "Iteration I" wheeled shank.

Iteration II
Iteration II adopts a minimalist approach compared to the original design, shown in Figure 3.8. The previous mount for the encoder and ball bearing are merged into the shank, significantly decreasing the volume. An additional internal cable channel is added to the shank, and both channel exits receive dedicated guides. Finally, the axle has been simplified into one 3D-printed element interfacing with the ball bearing, holding the magnet, and attaching to the wheel. Covers are not considered in this design.

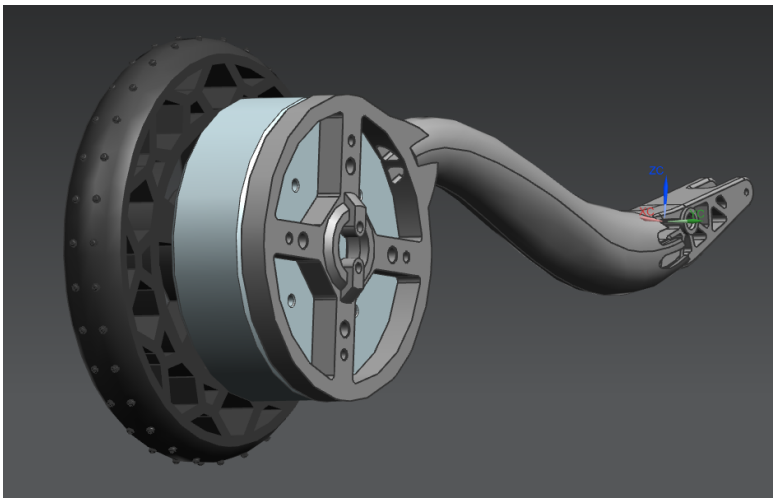

Figure 3.8: CAD rendering of the "Iteration II" wheeled shank.

Iteration IIa
Iteration IIa is nearly identical to the Iteration II design, with the primary difference being that it is scaled to fit the larger GM8112-80T [18] gimbal motor. This design was created due to concerns about the delayed delivery of the GL60 KV25 motors. The overall design retains the minimalist approach, integrated encoder and ball bearing mounts, additional internal cable channels with dedicated guides, and the simplified 3D-printed axle.

Iteration III
Iteration III is the final design for Minimal's wheeled shank, as shown in Figures 3.9 and 3.10.

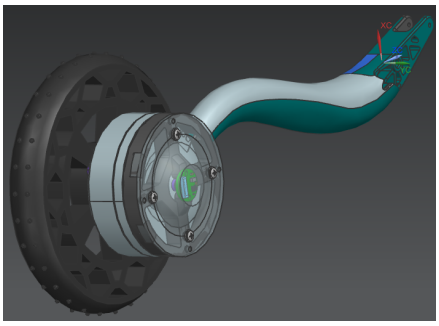

Figure 3.9: CAD rendering of the completed assembly.

Figure 3.10: The shank fully assembled.

Iteration III introduces several enhancements to the design. A protective cover for the encoder has been added to safeguard it from external elements. The design also features improvements to 3D-printability, ensuring more reliable and consistent production. Additionally, tolerances around the ball bearing have been refined for a better fit and smoother operation. These changes collectively enhance the durability and functionality of the shank assembly.

3.2.3 Detailed Design Information

This section describes some of the design features of the shank. For information on mass, inertia, and other physical properties, please refer to Section 5.1.2.

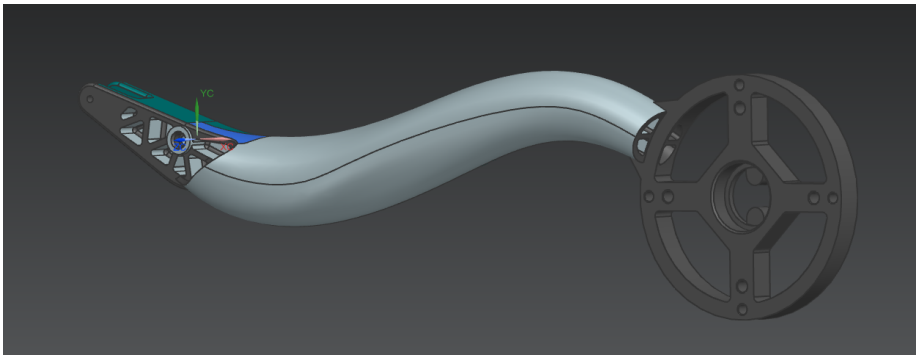

Figure 3.11: The redesigned shank includes motor and encoder attachment points, as well as the inlets of the two internal cable channels.

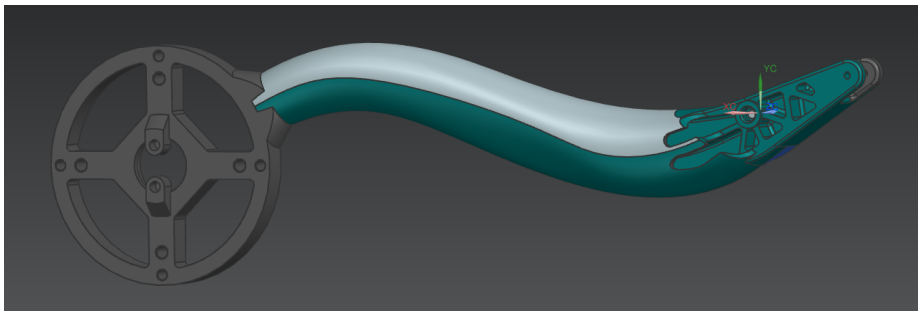

Figure 3.12: Visible on the back side is the encoder attachment point and the exits of the internal cable channels.

Minimal's new wheeled shank is illustrated in Figure 3.11. It retains the attachment points to the upper leg (thigh) on the left side of the figure. At the foot, a new attachment point secures the GL60 KV25 motor with M3 screws.
A central circular slot accommodates a 6x19x6 ball bearing, distributing load between the axle and the shank. The back side features a slot for a magnetic rotary encoder, as shown in Figure 3.12.
Internally, two channels route the three-phase power and encoder cables to the main body, while a cover plate over the encoder protects the cabling and sensitive electronics.
Due to the complex geometry of the shank and the nuances of 3D-printing, such as supports and infill, it was not feasible to conduct a finite element method (FEM) analysis. However, the produced prototypes, once assembled, displayed remarkable sturdiness and were more than sufficient for the intended use case.

Axle

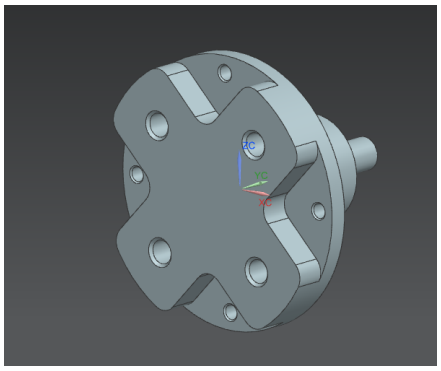

Figure 3.13: The front of the axle has attachment holes to the motor and wheel.

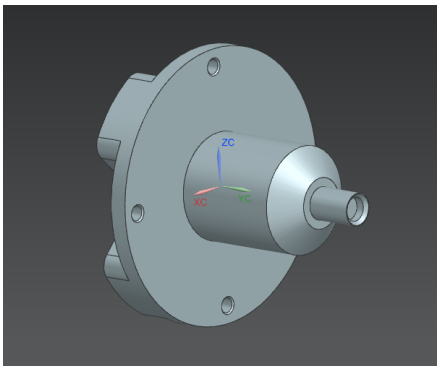

Figure 3.14: The back features the ball-bearing mount and a slot for the encoder's magnet.

The axle has three main functions:

- It serves as an attachment interface for the wheel and motor.
- It transfers the wheel's rotation through the motor's through-hole to the rotary encoder.
- It uses a ball-bearing, along with those in the GL60 KV25 motor, to absorb shocks during Minimal's walking.

The axle, as shown in Figure 3.13, features four holes designed for M3 thread inserts, which are embedded using a soldering iron. These threaded inserts facilitate the secure attachment of the wheel. Additionally, four M3 through holes allow for direct attachment of the axle to the motor.
Figure 3.14 illustrates the section of the axle that extends through the motor and partially into the shank. Visible in this figure is the surface where the 6x19x6 ball bearing is seated, providing load distribution between the axle and the shank. Also shown is a slot designed to house a magnet, which interacts with the magnetic rotary encoder for precise position tracking.

Cover

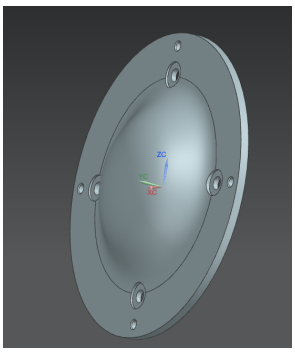

Figure 3.15: Front view of cover.

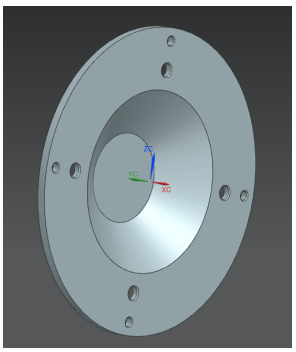

Figure 3.16: Back view of cover.

The cover, depicted in Figures 3.15 and 3.16, safeguards the encoder and encloses all internal wiring. It is secured using the same four M3 screws that attach the motor to the shank.

Combined Functionality
The section view of the assembly, as shown in Figure 3.17, reveals the internal configuration of components along the wheel axis. Most components are designed with multiple purposes in mind, such as the shank providing attachment points for the motor, cover, encoder, and ball-bearing.
The axle, highlighted in purple, passes through the motor's through-hole and utilizes a ball-bearing to absorb shocks during Minimal's walking.
The magnetic encoder, shown in green, and the corresponding diametrically magnetized magnet, shown in red, are both visible.

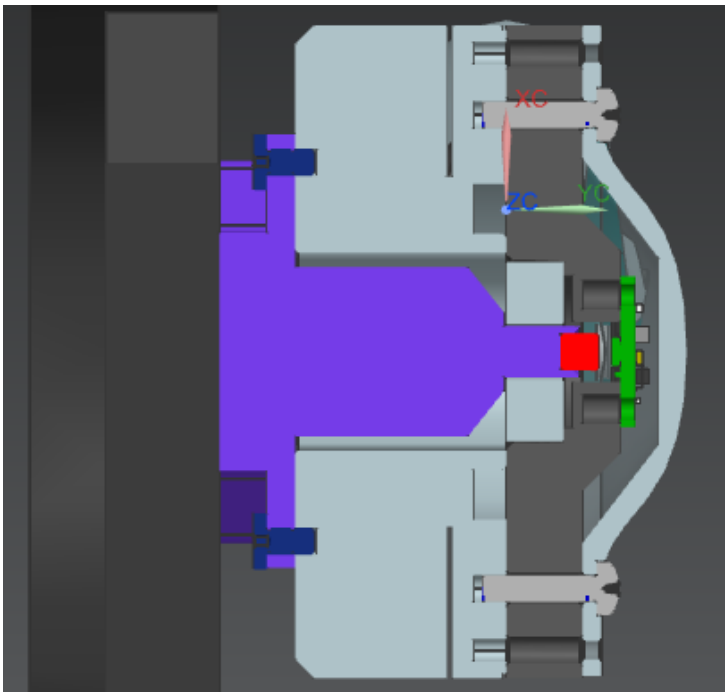

Figure 3.17: Section view of the assembly.

3.2.4 Electronics Configuration

In this section, I will explain the electronics configuration used to control the wheel motors of Minimal and turn it from a 12-DoF robot to a 16-DoF robot.

Power Control Board
The Nvidia Jetson Nano included in Minimal, it's brain, is not able to directly power the motors found on Minimal. Rather, a separate power control board (PCB) has to be used which turns actuator commands into three-phase current used by the motors. It also serves the purpose of receiving real-time information from the encoder and relaying it back to the Nvidia Jetson Nano. To accommodate four additional motors, four new PCBs are added to Minimal and conncected using serial linkage, described in the subsection "System Diagrams".
The power control board "MPSPCB 211025" is used for Minimal.

Integration of Power Control Board
Positioning the power control board was challenging due to the need for internal cable routing and PCB protection. Limited mounting spots without compromising the robot's range of motion were available.
After careful consideration, the PCB was placed on the upper thigh of Minimal, as illustrated in Figure [ADD ME]. This location minimally affected the range of motion and was conveniently close to an existing opening for electronics.
A custom casing was designed in Siemens NX and 3D-printed to secure and protect the PCB. It uses four M2 thread inserts and screws to hold the PCB. The casing itself is attached to Minimal's thigh with two M2 screws and a M2.5 screw. The casing provides sufficient internal space for cable routing and attaching heatsinks to the PCB's MOSFETs. The final printed casing is shown in Figures 3.18 and 3.19.

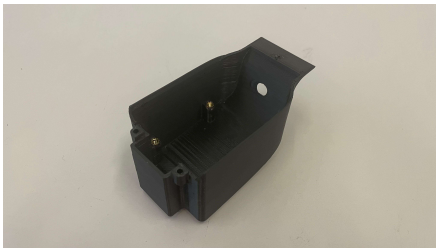

Figure 3.18: The PCB casing has a hole in the back to route cables.

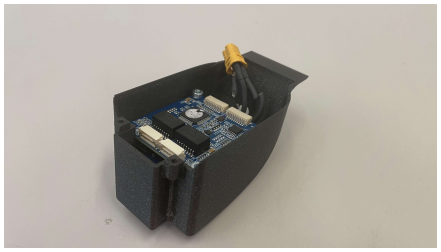

Figure 3.19: A dummy PCB is screwed into the casing.

Wiring Diagram

Figures 3.20 and 3.21 illustrate the concept of serial linkage used to connect the additional power control board to the existing circuitry. The wiring diagram in Figure 3.22 demonstrates the serial linkage for attaching the wheel electronics to Minimal in a modular fashion.

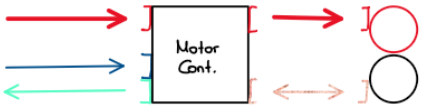

Figure 3.20: The regular PCB-Motor-Encoder configuration used on Minimal.

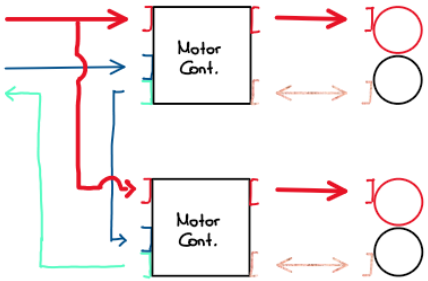

Figure 3.21: Using a serial linkage to add an additional PCB, motor, and encoder.

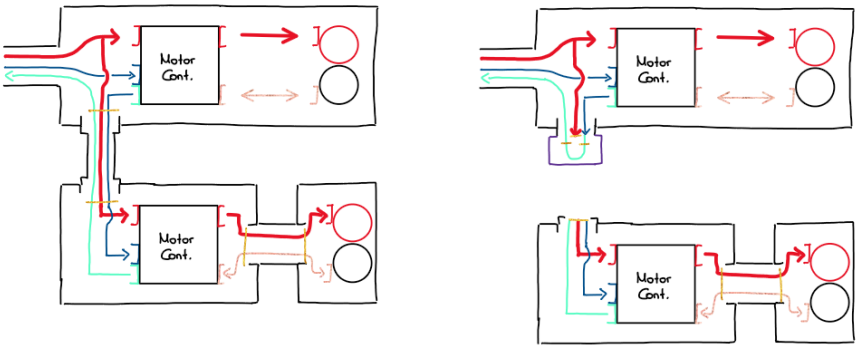

Figure 3.22: The wiring diagram demonstrates the modularity, allowing easy attachment and removal of the wheel motors.

Denoted as red and black circles are the motor and encoder respectively. Red arrows indicate power flow, either DC into the PCB or three-phase power into the motor.

Test Stand
A small test stand was 3D-printed and constructed in order to calibrate the power control board. It includes the same mounting points as the shank and is shown fully assembled in Figure.

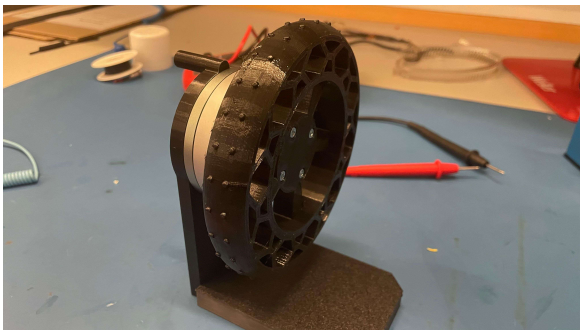

Figure 3.23: Assembled test stand with motor, axle, ball-bearing, magnet, and wheel attached.

3.2.5 Production

Various 3D printers were used to prototype the shank, axle, cover, and PCB enclosure. Two Creality Ender V3 KE (Shenzhen Creality 3D Technology Co., Ltd.) 3D printers were used to produce the final shanks, covers, and axles. Notably, two of the four shanks are produced mirrored for the robot.
A Prusa i3 MK3 (Prusa Research a.s.) 3D printer was used to make the PCB casing.
All parts were printed using regular PLA and at a layer height of 0.2mm.
Figure 3.24 depicts four completed shanks and the test stand.

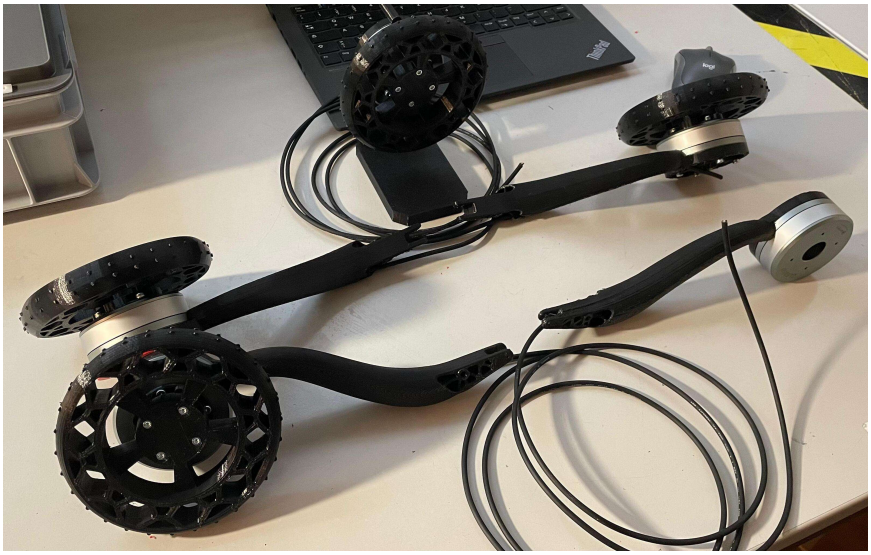

Figure 3.24: Three assembled and one partially-assembled shank, together with the test stand.

Chapter 4

Policy Training

4.1 Reinforcement Learning Environment

4.1.1 Legged Gym

Developing robust locomotion policies for robotic systems is a challenging endeavor and an intense focus of current research. Deep reinforcement learning has emerged as a powerful method to train robust policies, enabling robots to handle variations in terrain, dynamic obstacles, and multi-task goals [24].

For training Minimal's locomotion policy, we use the Robotic Systems Lab's "Legged Gym" [25], a reinforcement training framework that leverages Nvidia's high-fidelity physics simulator IsaacGym [26].

Several papers have highlighted the success of using these simulation environments for training robust locomotion policies. For instance, the work by Miki et al. (2022) [4] demonstrates robust integration of exteroceptive and proprioceptive perception for legged robots, while Lee et al. (2024) [14] developed a versatile locomotion controller for a wheeled-legged system in urban environments.

4.1.2 Updating Robot Representation

Legged Gym uses the Unified Robotics Description Format (URDF) to describe robot models for simulation. An existing URDF for Minimal was modified to accurately reflect the new design and components. A rotary joint and corresponding link was added to the shank to denote the wheel. Updated STL geometry from the shank and wheel CAD designs were added in addition to revised collision boxes.

Both the masses and inertia values of the shank and wheels were updated to improve the dynamic accuracy of the model. The inertia of the shank was derived from physical pendulum tests, while the inertia of the wheels was calculated used CAD software. More information on this can be found in the Appendix.

While the HAA, HFE, and KFE actuators of Minimal remained unchanged, a new actuator for the wheel was configured into legged gym, based on the specifications of the chosen GL60 KV25 motor. This motor was configued for velocity control to better match the intended driving functionality.

Figures 4.1 and 4.2 illustrate the original and updated URDF models, respectively.

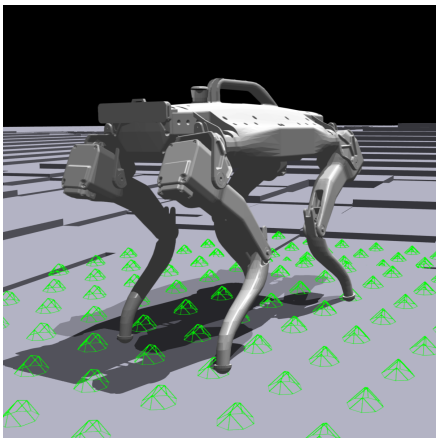

Figure 4.1: The original Minimal URDF displayed in legged gym.

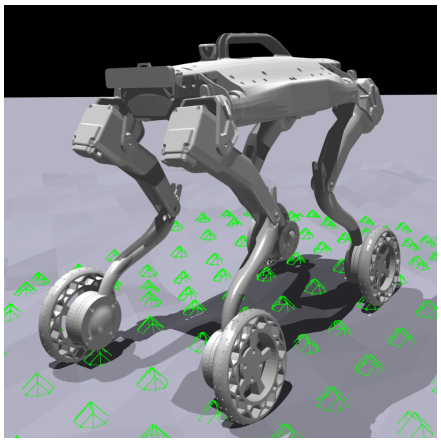

Figure 4.2: The URDF was updated to account for the new joints, geometries, weights, and moments of inertia.

4.1.3 Configuration and Training

Neural Network

Minimal's locomotion controller is represented by two multilayer perceptrons (MLP) in an Actor-Critic model as shown in Figures 4.3 and 4.4. The actor generates actions based on the current proprioceptive observations and commanded velocities, and is eventually deployed on the real robot. The critic evaluates the actions taken by the actor and estimates the value function, providing feedback to the actor on the quality of actions taken. Combined, the model is able to learn from both immediate rewards and future potential rewards, which is beneficial for learning locomotion policies.

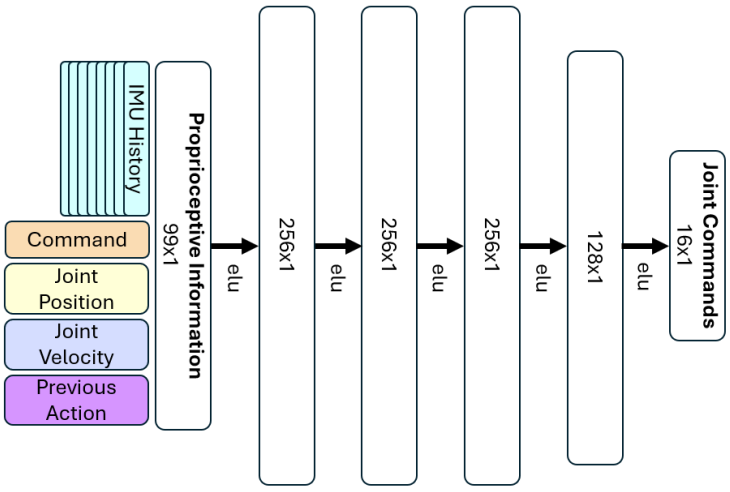

Figure 4.3: Architecture of Actor MLP.

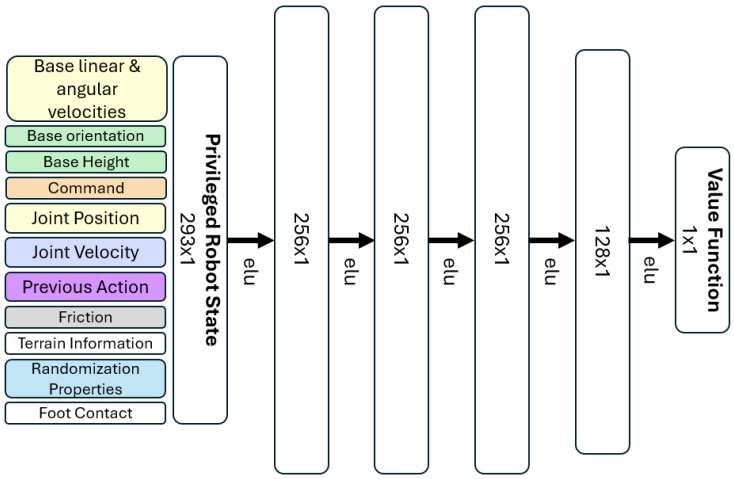

Figure 4.4: Architecture of Critic MLP.

Simulation Setup
The training involves 4096 Minimal robots placed into the simulation environments. The robots are told to maximize select reward functions, such as following velocity commands and not falling over. The agents "learn" by using a Proximal Policy Optimization algorithm and leveraging GPU parallelization for simulation, training, and inference.

Terrain Curriculum
Curriculum training is implemented to progressively challenge the robots and teach the locomotion policy to cross increasingly difficult terrain. The terrain generation and curriculum follow the same methodology as described in Rudin et al. (2018) [25] where the complexity of the terrain is incrementally increased as the robots demonstrate proficiency. Figures 4.5 and 4.6 depict this process.

Randomization
To make Minimal's locomotion policy more robust against external disturbances, randomization techniques are applied to the robot in simulation, including:

- The starting position of the robot is randomized within a 1-meter radius.
- External pushes are applied to Minimal every 10 seconds with a maximum force of 2 Newtons and a maximum torque of 0.4 Newton-meters.
- The friction between robot and environment is varied.
- The base mass of Minimal can vary between ± 0.5 kg.
- Proprioceptive observations are affected by sensor noise.

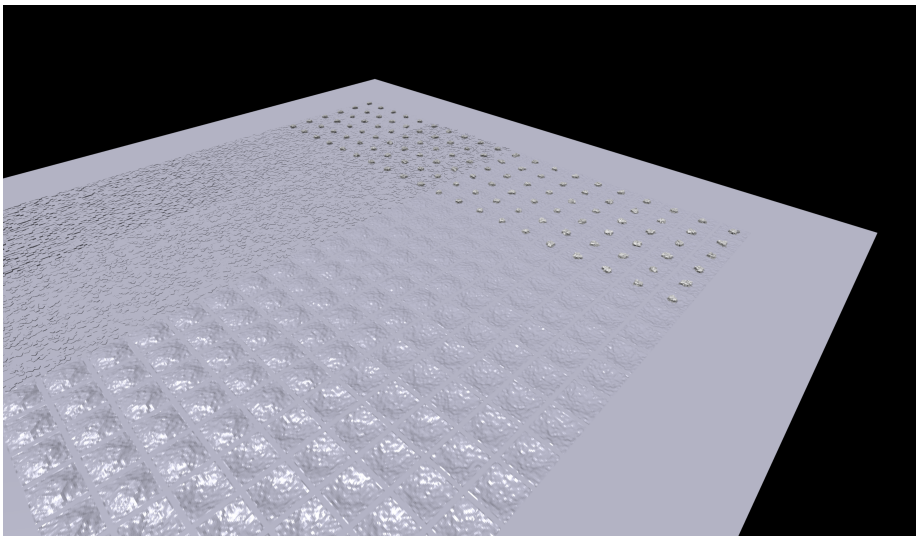

Figure 4.5: At the start of training, robots are placed in the easiest terrain zones.

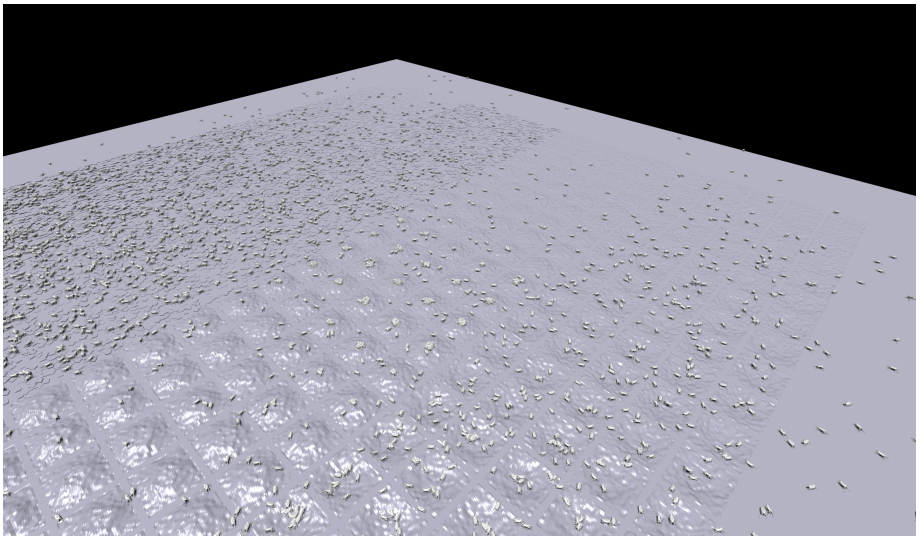

Figure 4.6: As movement becomes more proficient, robots spawn in more challenging terrain.

4.2 ROS Implementation

Minimal's software runs on a Nvidia Jetson Nano using ROS2. The implementation was updated from ROS2 Galactic to ROS2 Iron to leverage new features like the rclcpp-events-executor. The configuration was modified to control the new motors and observe the rotational encoders.
The deep learning inference framework was adjusted to handle 16 DoF outputs for testing the new locomotion policy in ROS2. A simple ROS2 navigation node was developed to facilitate this testing. This node subscribes to position and orientation targets from the Gazebo simulator. A PI controller computes the error between the intended and actual positions/orientations and publishes velocity commands to correct the robot's movement. The results of this simple controller are depicted in Figures 4.7 and 4.8.

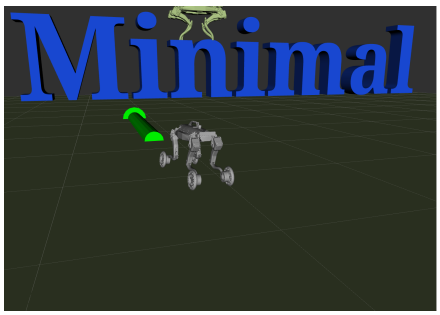

Figure 4.7: Minimal receives a position target (green arrow).

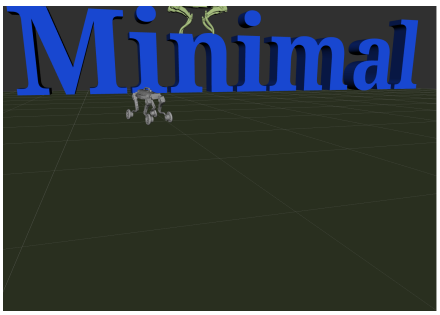

Figure 4.8: Minimal uses the locomotion policy to drive to the target and stops.

Chapter 5

Results and Discussion

5.1 Results

5.1.1 Test Stand

The test stand is a platform to validate the correct operation of the motor and encoder. It consists of the following parts:

- 1x 3D-printed base
- 1x 3D-printed motor mount
- 1x 3D-printed axle
- 1x TPU wheel
- 1x GL60 KV25 gimbal motor
- 1x 626-2RSH 6x19x6 bearing
- 4x4mm diametrical cylinder magnet
- MA732 angular encoder [27]
- 6x M3x5.7mm thread inserts
- 2x M2x2.5mm thread inserts
- 4x M3x14mm screws
- 6x M3x10mm screws
- 4x M3x6mm screws
- 2x M2x4mm screws
- Three-phase motor cabling
- Encoder cabling

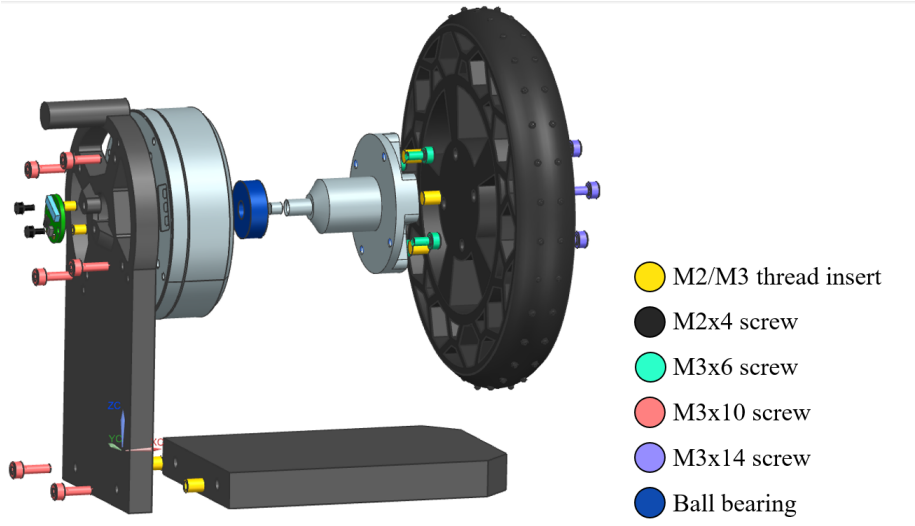

Figure 5.1: Exploded view of the test stand assembly.

5.1.2 Wheeled Shank

The final wheeled shank consists of the following parts:

- 1x 3D-printed shank*
- 1x 3D-printed axle
- 1x 3D-printed cover
- 1x TPU wheel
- 1x GL60 KV25 gimbal motor
- 1x 626-2RSH 6x19x6 bearing
- 4x4mm diametrical cylinder magnet
- MA732 angular encoder [27]
- 4x M3x5.7mm thread inserts
- 2x M2x2.5mm thread inserts
- 4x M3x14mm screws
- 4x M3x12mm screws
- 4x M3x6mm screws
- 2x M2x4mm screws
- Three-phase motor cabling
- Encoder cabling

**Note: For the 3D-printed shank, two of the four shanks had to be printed as a symmetric flip to ensure proper assembly.*

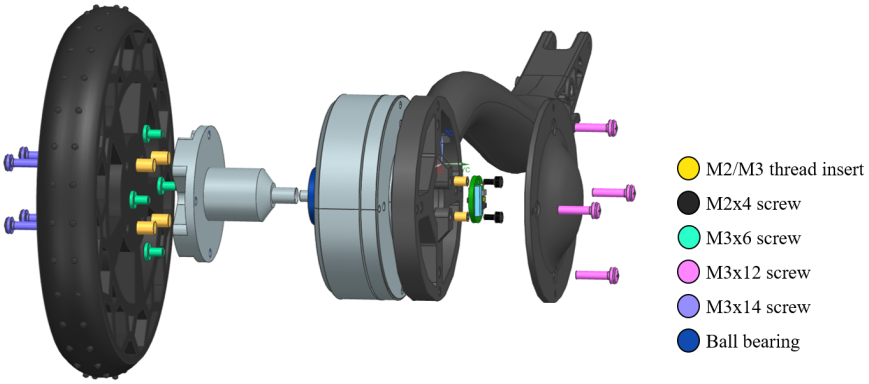

Figure 5.2: Exploded view of the wheeled shank assembly.

Table 5.1: Physical Parameters of the Final Shank Design

Parameters	Values		
	Weight	**Dimensions**	**Max Torque**
Value	0.3412	310 x 126 x 66	2.0
Units	kg	mm x mm x mm	Nm
	Inertia I_{xx}	**Inertia I_{yy}**	**Inertia I_{zz}**
Value	0.002	0.001	0.003
Units	kg·m^2	kg·m^2	kg·m^2
	Max Speed	**Max Speed**	**Max Current @18V**
Value	350	2.2	4.2
Units	rpm	m/s	A

5.1.3 Policy Results

Several reinforcement learning policies were developed and tested to achieve robust locomotion for the Minimal robot. After extensive evaluation, the best-performing policy was selected based on its overall reward, stability, and ability to follow velocity commands. This section presents the key metrics and results for the selected policy.

Training Performance
Selected rewards of Minimal on Wheels during the training process is shown in Figures 5.3 and 5.4. The plot suggests that locomotion is successfully training within approximately 3,000 steps and sees little increase when trained to 11,000 steps.

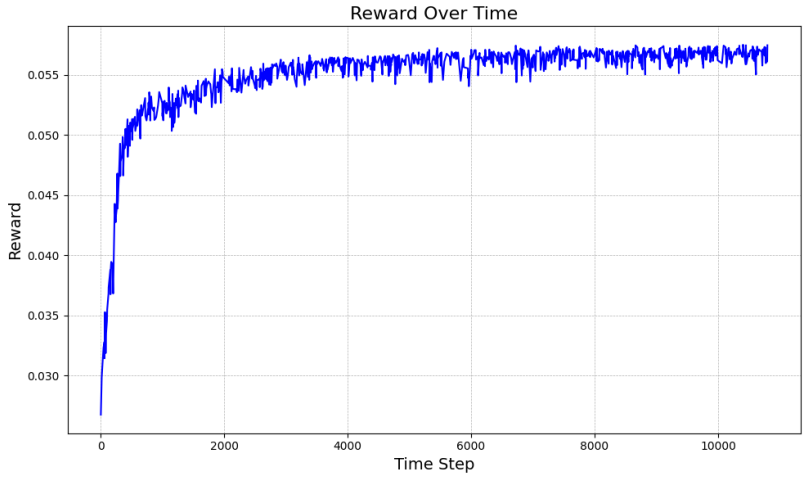

Figure 5.3: Reinforcement learning rewards of Minimal on Wheels over 11,000 time steps.

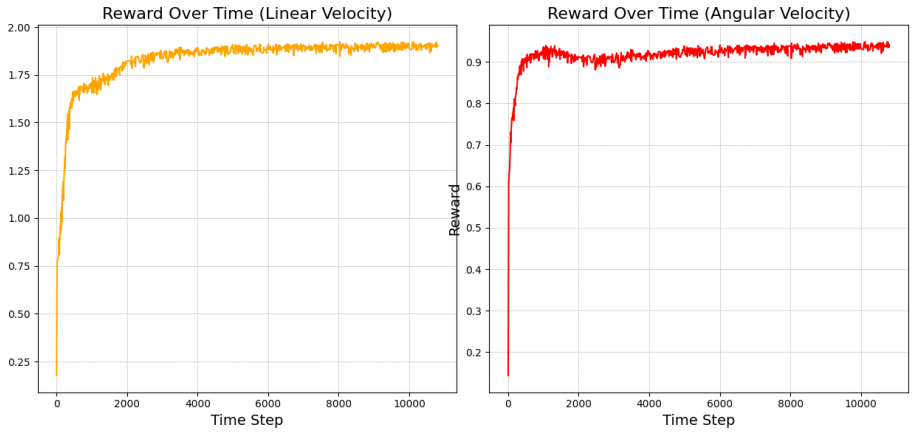

Figure 5.4: Specific reward for linear and angular velocity tracking over 11,000 time steps.

Locomotion Performance

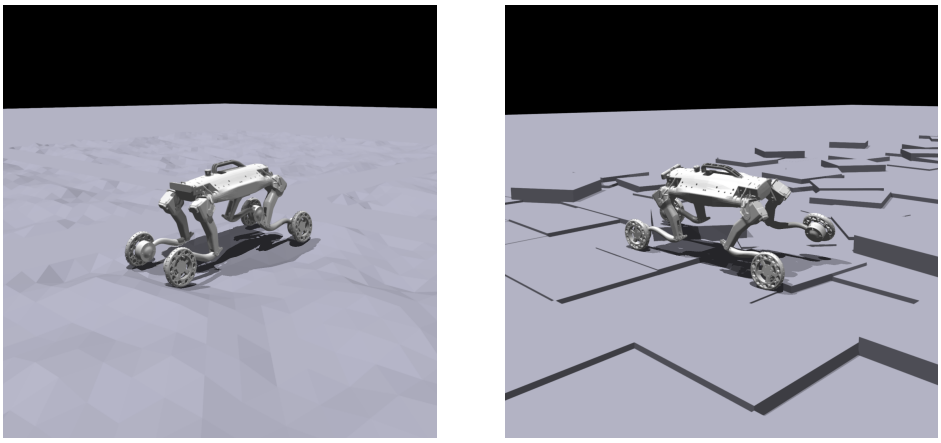

(a) (b)

(c) (d)

Figure 5.5: Minimal's locomotion performance: (a) pure driving motion, (b) stepping motion for sideways movement and overcoming obstacles, (c) wheels maintaining ground contact, (d) hybrid driving and side-stepping motion.

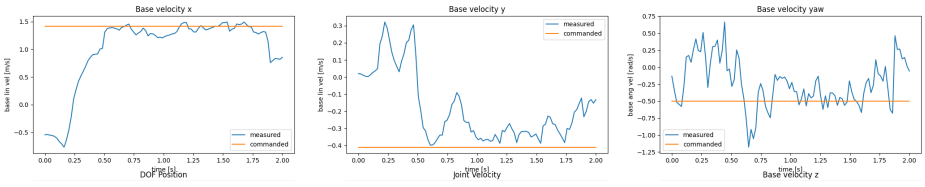

Figure 5.6: The policy tracking an extreme velocity command.

Minimal on Wheels effectively leverages its new degrees of freedom, learning different locomotion patterns for different tasks, seen in Figure 5.5. It is also able to accurately track simultaneous x, y, and yaw velocity commands over bumpy, blocky, and slippery terrain. Shown in Figure 5.6 is the case of an extreme reference velocity close to the policy's maximum. Minimal quickly accelerates to the required forward

velocity of $1.5m/s^2$ and begins concurrently side-stepping to match the other two velocity commands.

5.2 Discussion

5.2.1 Hardware Discussion

5.2.2 Software Discussion

This worked well, this is why it worked well. Explanation of results.

Chapter 6

Outlook

Chapter 7

Conclusion

Bibliography

[1] Y. Gao, B. Su, L. Jiang, and F. Gao, "Multi-legged robots: progress and challenges," *National Science Review*, vol. 10, 5 2023.

[2] Y. Gong, G. Sun, A. Nair, A. Bidwai, R. CS, J. Grezmak, G. Sartoretti, and K. A. Daltorio, "Legged robots for object manipulation: A review," 3 2023.

[3] M. Sombolestan and Q. Nguyen, "Adaptive force-based control of dynamic legged locomotion over uneven terrain," 7 2023.

[4] T. Miki, J. Lee, J. Hwangbo, L. Wellhausen, V. Koltun, and M. Hutter, "Learning robust perceptive locomotion for quadrupedal robots in the wild," p. 2822, 2022.

[5] M. Bjelonic, V. Klemm, J. Lee, and M. Hutter, "A survey of wheeled-legged robots," vol. 530 LNNS, 2023.

[6] N. Corporation, "Nvidia jetson nano," n.d., accessed: 2024-07-04.

[7] T-Motor, "Mn4006 antigravity type 4-6s uav motor kv380," n.d., accessed: 2024-07-04.

[8] V. Klemm, A. Morra, C. Salzmann, F. Tschopp, K. Bodie, L. Gulich, N. Küng, D. Mannhart, C. Pfister, M. Vierneisel, F. Weber, R. Deuber, and R. Siegwart, "Ascento: A two-wheeled jumping robot," 5 2020.

[9] S. Wang, L. Cui, J. Zhang, J. Lai, D. Zhang, K. Chen, Y. Zheng, Z. Zhang, and Z. P. Jiang, "Balance control of a novel wheel-legged robot: Design and experiments," vol. 2021-May. Institute of Electrical and Electronics Engineers Inc., 2021, pp. 6782–6788.

[10] B. Dynamics, "Introducing handle," YouTube, 2017.

[11] M. Bjelonic, C. D. Bellicoso, Y. de Viragh, D. Sako, F. D. Tresoldi, F. Jenelten, and M. Hutter, "Keep rollin' - whole-body motion control and planning for wheeled quadrupedal robots," 9 2018.

[12] I. Zournatzis, K. Koutsoukis, K. Machairas, A. Kecskeméthy, and E. G. Papadopoulos, *Maera: A Hybrid Wheeled-Legged Robot Designed for Research and Education*, 2021, pp. 247–261.

[13] U. Robotics, "Unitree b2-w," 2024, accessed: 2024-07-04.

[14] J. Lee, M. Bjelonic, A. Reske, L. Wellhausen, T. Miki, and M. Hutter, "Learning robust autonomous navigation and locomotion for wheeled-legged robots," 2024.

[15] C. Lee, S. Kwak, J. Kwak, and S. Oh, "Generalization of series elastic actuator configurations and dynamic behavior comparison," *Actuators*, vol. 6, 9 2017.

[16] G. A. Pratt and M. M. Williamson, “Series elastic actuators.”

[17] T-Motor, “T-motor the safer propulsion system,” https://uav-en.tmotor.com/, 2024, accessed: 2024-05-11.

[18] iFlight Innovation Technology Ltd., “iflight store,” https://shop.iflight.com/, 2024, accessed: 2024-05-11.

[19] T-Motor, “Motor mapping visualization,” https://store.tmotor.com/product/gl60-out-running-gimbal-motor.html, 2024, accessed: 2024-07-04.

[20] S. Sato, T. Yamaguchi, K. Shibata, T. Nishi, K. Moriyasu, K. Harano, and K. Hokkirigawa, “Dry sliding friction and wear behavior of thermoplastic polyurethane against abrasive paper,” *Biotribology*, vol. 23, 9 2020.

[21] L. MATWEB, “Material property data,” https://matweb.com/search/datasheet.aspx?matguid=2fe782a31c4b4bed984b49651762b086&ckck=1, 2024, accessed: 2024-07-05.

[22] R. Technologies, “Non-pneumatic (airless) tire,” https://www.oemoffhighway.com/drivetrains/tracks-tires/tires-wheels/tracks-tires/product/10343599/resilient-technologies-nonpneumatic-airless-tire, 2024, accessed: 2024-07-05.

[23] S. Wang, S. Tang, C. He, and Q. Wang, “Cyclic deformation and fatigue failure mechanisms of thermoplastic polyurethane in high cycle fatigue,” *Polymers*, vol. 15, 2 2023, contains valuable information on the cyclic loading of TPU, in particular an analytical expression for Basquin’s formula providing the S-N curve of TPU.

[24] J. Ibarz, J. Tan, C. Finn, M. Kalakrishnan, P. Pastor, and S. Levine, “How to train your robot with deep reinforcement learning: lessons we have learned,” *International Journal of Robotics Research*, vol. 40, pp. 698–721, 4 2021.

[25] N. R. E. Zurich, D. H. E. Zurich, P. Reist, and M. H. E. Zurich, “Learning to walk in minutes using massively parallel deep reinforcement learning.”

[26] J. Liang, V. Makoviychuk, A. Handa, N. Chentanez, M. Macklin, and D. Fox, “Gpu-accelerated robotic simulation for distributed reinforcement learning,” 10 2018.

[27] M. P. Systems, “Ma732,” https://www.monolithicpower.com/en/ma732.html, 2024, accessed: 2024-07-20.

[28] C. GmbH, “Datenblatt zu type 626/c3 skf - 626 c3 skf (ungefettet)(rillenkugellager),” https://www.kugellager-shop.net/626-c3-skf-rillenkugellager-6x19x6-mm-19x6x6mm.html, 2024, accessed: 2024-04-25.

[29] A. Bearings, “6700zz thin section bearings: Metric series ball bearing,” https://www.astbearings.com/catalog/thin_section_metric/6700ZZ, 2024, accessed: 2024-07-11.

Appendix A

Appendix A

A.1 Motor Weight

The wheel motor attached to the bottom of Minimal's shank should be lightweight enough to avoid significantly hindering the robot's movement. Given Minimal's actuator configuration, the KFE joint bears the brunt of this design change, as it must now lift the shank and the motor assembly attached to the end of the shank. Initial calculations, followed by validation in the Legged Gym physics environment, confirmed that the 'GL60 KV25' is suitably lightweight.

Initial Estimates
Minimal's KFE joint is powered by a T-Motor MN4006 with a maximum torque of $0.5Nm$ with a combined worm gear and crank-slider mechanism resulting in an effective gear ratio between 5 and 7. Figure A.1 illustrates the setup of the problem.

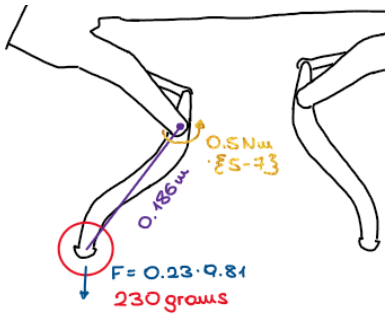

Figure A.1: A simplified sketch of the isolated KFE dynamics.

Assuming a worst-case scenario of the shank being horizontal, as well as a gear ratio of 5, the dynamics problem is:

$$I\ddot{\theta} = \sum M \tag{A.1}$$

$$(m_{motor} \cdot r^2)\ddot{\theta} = M_{KFE} \cdot n - m_{motor} \cdot 9.81 \cdot r \tag{A.2}$$

$$\ddot{\theta} = \frac{M_{KFE} \cdot n - m_{motor} \cdot 9.81 \cdot r}{m_{motor} \cdot r^2} \tag{A.3}$$

Using known data from Minimal and the motor:

- Maximum moment produced by KFE motor: $M_{KFE} = 0.5\text{Nm}$

- Lower estimate for KFE gear ratio: $n = 5$
- Mass of GL60 KV25 motor: $m_{motor} = 0.23\text{kg}$
- Distance between shank joint and GL60 KV25 motor: $r = 0.186\text{m}$

$$\ddot{\theta} = 261.443 rad/s^2 \tag{A.4}$$

This angular acceleration of the shank is deemed sufficient for the use case of driving and walking.

Legged Gym Validation
Following the implementation of Minimal on Wheels in legged gym, described in Section 4.1.2, Minimal exhibited good agility and movement in testing environments, seen in Figure A.2.

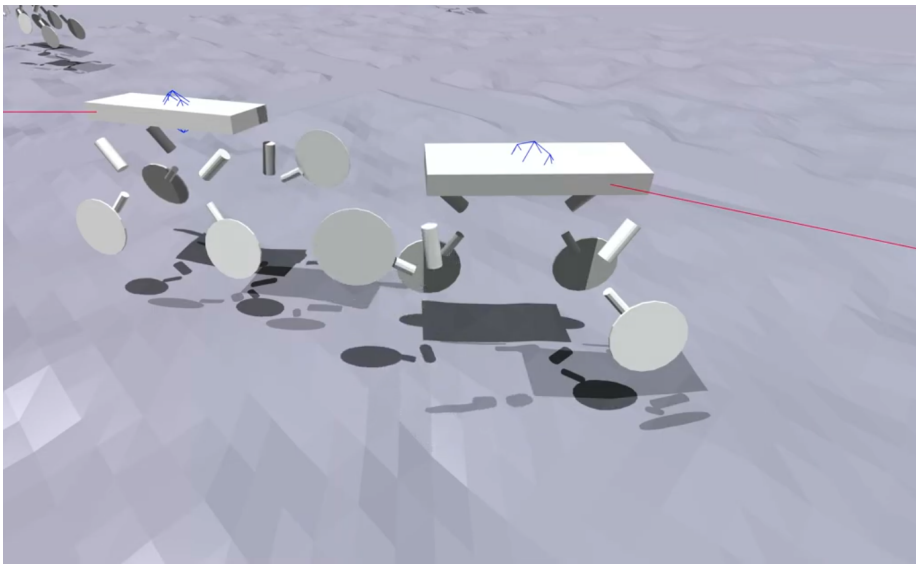

Figure A.2: Minimal testing its joints. The regular view replaced by collision body view.

A.2 Ball Bearing Calculations

The GL60 KV25 motor chosen for Minimal on Wheels internally contains a ball bearing of type 6705ZZ [19]. While this ball bearing is sufficient to sustain radial loads, it cannot take moments along the axle.

Therefore, it was decided to add an additional ball bearing along the axle, as sketched in Figure A.3. The 626-2RSH 6x19x6 ball bearing was chosen due to its strength yet compact size.

Data for both was gathered for the 6700ZZ and 626-2RSH ball bearings from CQ GmbH [28] and AST Bearings [29] respectively.

Table A.1: Properties of the Ball Bearings Used

Property	**6700ZZ**	**626-2RSH 6x19x6**
Cr	855	$2340N$
Cor	435	$950N$
n	$15000min^{-1}$	$24000min^{-1}$

It is difficult to estimate the forces on the axle resulting from shocks and the alleviation through the damping of the wheels. However, some basic longevity estimates can be made by assuming dynamic loads.

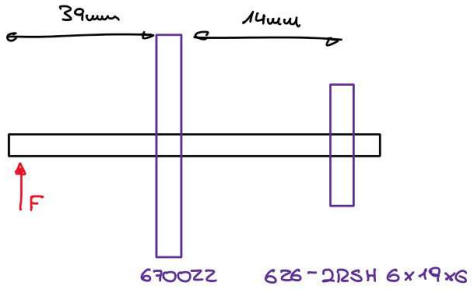

Figure A.3: A sketch of the bearing configuration on the axle.

Regular Driving
Assuming a "heavy" Minimal robot of 5kg weight during normal driving operations, each wheel is affected by $16.7N$ of force. Decomposing this force into force on the 6700ZZ bearing (A) and 626-2RSH bearing (B) results in $F_A = 63.22N$ and $F_B = 46.52N$.
Using the equation from the L10 life theory:

$$L_{10} = (\frac{Cr}{P})^3 \cdot 10^6 \tag{A.5}$$

...the bearings have a 90% survival chance up to $n_A = 2.473 \cdot 10^9$ and $n_B = 1.272 \cdot 10^{11}$ revolutions respectively.

Heavy Load
To approximate a strong load on the axle, such as during stomping, an equivalent force of $100N$ on each wheel is chosen. This is decomposed into $F_A = 378.5N$ and $F_B = 278.6N$. Using the L10 life theory, the bearings have a 90% survival chance up to $n_A = 1.15 \cdot 10^7$ and $n_B = 5.93 \cdot 10^8$ revolutions respectively.
For the purposes of this prototype, this survival time is more than sufficient. Under these loads, it is more likely other parts of the motor assembly fail before the ball-bearings do.

Appendix B

Appendix B

B.1 Datasheet of motors compared

Table B.1: Comparison of Different Motors

Name	Torque (Nm)	Power (W)	Current (A)	Voltage (V)	Weight (g)	Price ($)	Family
MN4006 KV380	0.4	360	15	24	68	75	MN
MN5008 KV170	0.87	687	15	47	128	90	MN
MN5008 KV340	0.89	754	33.50	22.5	128	90	MN
MN6007 KV320	1.3	908	38.31	23.7	180	120	MN
G35 KV100	0.45	72	4.5	16	159	55	G
G40 KV70	0.7	80	5	16	183	73	G
G40 KV210	2.0	720	45	16	163	73	G
G60 KV55	2.25	120	5	24	364	109	G
GL35 KV100	0.45	72	4.5	16	90	55	GL
GL40 KV70	0.7	80	5	16	107	73	GL
GL40 KV210	2.1	720	45	16	107	73	GL
GL60 KV25	2.25	100.8	4.2	24	230	109	GL
GM110-8T	1.18	40	2	20	534	170	GM
GM8112-80T	0.883	40	2	20	428	130	GM
GM110-10	1.4	40	2	20	532	190	GM

Data was collected from the T-Power [17] and iFlight [18] websites respectively.